CHAPTER 2

THEORY AND LITERATURE SURVEY

2.1 Composite Materials

Composites are the result of embedding high strength, high stiffness fibers of one material in a surrounding matrix of another material. The fibers of interest for composites are generally in the form of either single fibers about the thickness of the human hair or multiple fibers twisted together in the form of a yarn or tow. When properly produced, these fiber-usually of a nonmetallic material such as carbon, silicon carbide, boron, or alumina-can have very high values of strength and stiffness. As a result of work that started in the United States in the early 1950s, there are available to us thin, continuous fibers of a variety of materials, together with the manufacturing capability to produce them on a continuous basis. In addition to continuous fibers, there are also varieties of short fibers, whiskers, platelets, and particulates intended for use in discontinuous reinforced composites. Fiber-reinforced composite materials consist of fibers of high strength and modulus embedded in or bonded to a matrix with distinct interfaces (boundaries) between them. In this form, both fibers and matrix retain their physical and chemical identities, yet they produce a combination of properties that cannot be achieved with either of the constituents acting alone. In general, the fibers are the principal load carrying members, whereas the surrounding matrix keeps them in the desired location and orientation, act as a load transfer medium between them, and protects them from environmental damages due to elevated temperature or humidity, for example. Thus, even though the fibers

provide reinforcement for the matrix, the latter also serves a number of useful functions in a fiber-reinforced composite material. The principal fibers in commercial use are various types of glass and carbon, as well as, Kevlar and those mentioned previously. All these fibers can be incorporated into a matrix either in continuous lengths or in discontinuous (chopped) lengths. The matrix material may be a polymer, a metal, or a ceramic. Various chemical combinations, composition and microstructure arrangements are possible in each matrix category.

The most common form in which fiber-reinforced composites are used in structural applications is called a laminate. Laminates are obtained by stacking number of thin layers of fibers and matrix and consolidating them into the desired thickness. Fiber orientation in each layer, as well as the stacking sequence of various layers, can be controlled to generate a wide range of physical and mechanical properties for the composite laminate [6].

In mechanical terms, nanocomposites differ from conventional composite materials due to the exceptionally high surface to volume ratio of the reinforcing phase and/or its exceptionally high aspect ratio. The reinforcing material can be made up of particles (e.g. minerals), sheets (e.g. exfoliated clay stacks) or fibers (e.g. carbon nanotubes or electrospun fibers). The interface area between the matrix and reinforcement phase(s) is typically an order of magnitude greater than for conventional composite materials. The matrix material properties are significantly affected in the vicinity of the reinforcement. Ajayan et al. [25] note that with polymer nanocomposites, properties related to local chemistry, degree of thermoset cure, polymer chain mobility, polymer chain conformation, degree of polymer chain

ordering or crystallinity can all vary significantly and continuously from the interface with the reinforcement into the bulk of the matrix.

2.2 Matrix Phase: Thermoset Resin

Epoxy resin will retain their dominant position in the thermoset resin sector over the next 5 years despite competition from other resins that offer superior high temperature performance. Although a number of factor serve to inhibit the development of radically new chemical systems, epoxy resin suppliers will continue to introduce innovations in response to the demand for improve process ability and performance. Concern regarding health and the costs involved in obtaining the necessary approval and registration of truly new chemical systems are major barriers to radical departures from established chemistry. Starting materials for epoxy matrix are low-molecular-weight organic liquid resins containing a number of epoxide groups, which are three-membered rings consisting of one oxygen atom and two carbon atoms.

Epoxy matrix, as a class, has the following advantages over other thermoset matrices:

a) A wide variety of properties because a large number of starting materials, curing agent, and modifiers are available

b) An absence of volatile matters during cure

c) Low shrinkage during cure

d) Excellent resistance to chemicals and solvent

e) Excellent adhesion to a wide variety of fillers, fibers, and other substrates

f) High or low strength and flexibility

g) Resistance to creep and fatigue

h) Good electric properties

i) Solid or liquid resins in the uncured state

j) A wide range of curative options.

The principle disadvantages are its relatively high cost and long cure times, as well as

a) Resins and curative somewhat toxic in uncured form

b) Heat distortion point lowered by moisture absorption

c) A change in dimensions and physical properties as a result of moisture absorption

d) Use (dry) limited to about 200 °C upper temperature

e) Difficult to combine toughness and high-temperature resistance

f) A high thermal coefficient of expansion

g) A high degree of smoke liberation in a fire

h) May be sensitive to ultraviolet light degradation.

These resins cost more than polyesters and do not have the high-temperature capability of BMIs or PIs; but because of their advantages, they are used widely. The epoxy resins are capable of upper service temperatures in the range 125 - 175°C, depending on the composition. The toughened versions of epoxy resins are tailored for use up to 125°C, whereas the more rigid epoxy compositions are capable of service temperatures up to 175°C. The significant differences in the properties of the various epoxy materials are in the moduli, strains to failure, and glass transition temperatures. The glass transition temperature, which controls the use temperature of the various epoxy materials, is high (247°C) for the brittle epoxies and much lower for the toughened epoxies (76 and 185°C). Therefore, it is clear that one compromises the use of temperature of gain toughness in these resin materials [6].

2.3 Reinforcement Phase

Reinforcements can be divided into two major groups, particulates, and fibers. Fiber reinforcements can be further divided into continuous and discontinuous fibers.

2.3.1 Carbon Nanotubes (CNTs)

The current huge interest in carbon nanotubes is a direct consequence of the synthesis of buckminsterfullerene, C-60 , and other fullerenes, in 1985. The discovery that carbon could form stable, ordered structures other than graphite and diamond stimulated researchers worldwide to search for other new forms of carbon. The search was given new impetus when it was shown in 1990 that C60 could be produced in a simple arc-evaporation apparatus readily available in all laboratories. It was using such an evaporator that the Japanese scientist Sumio Iijima discovered fullerene-related carbon nanotubes in 1991. The tubes contained at least two layers, often many more, and ranged in outer diameter from about 3 nm to 30 nm. They were invariably closed at both ends. A transmission electron micrograph of some multiwalled nanotubes is shown in the fig. 2.1. In 1993, a new class of carbon nanotube was discovered, with just a single layer. These single-walled nanotubes are generally narrower than the multi-walled tubes, with diameters typically in the range 1-2 nm, and tend to be curved rather than straight. The image on the right shows some typical single-walled tubes. It was soon established that these new fibers had a range of exceptional properties, and this sparked off an explosion of research into carbon nanotubes. It is important to note, however, that nano-scale tubes of carbon, produced catalytically, had been known for many years before Iijima's discovery. The main reason why these early tubes did not excite wide interest is that they were structurally

rather imperfect, so did not have particularly interesting properties. Recent research has focused on improving the quality of catalytically produced nanotubes.

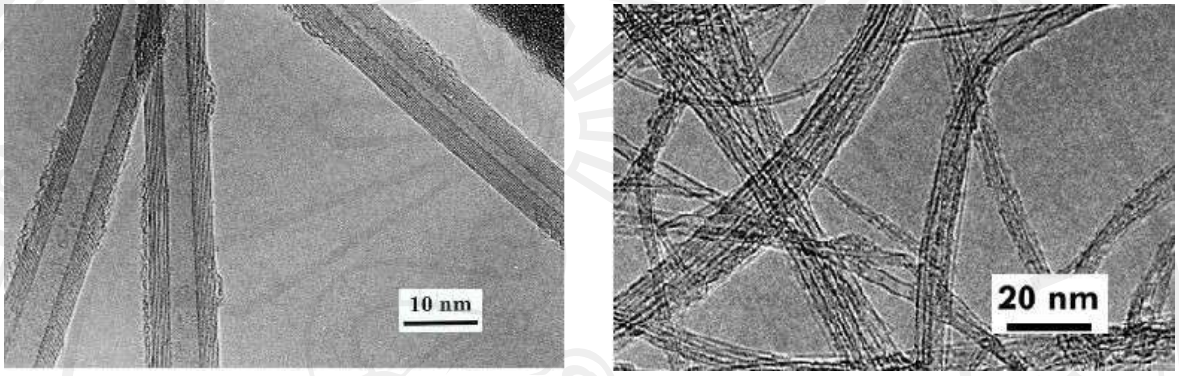

Figure 2.1 Transmission electron micrograph of some multiwalled nanotubes [26]

1) Structure of carbon nanotubes

The basic structure of CNTs is comprised of sp^2 carbons, with each atom joined to three neighbors, as in graphite. The tubes can therefore be considered as rolled-up graphene sheets. To describe this structure, a chiral vector is defined as C_h = na1+ ma2, where a1 and a2 are unit vectors for the hexagonal lattice of the graphene sheet, n and m are integers, along with a chiral angle θ, which is the angle of the chiral vector with respect to the x direction (fig 2.2). Using this (n, m) scheme, the three types of nanotubes is characterized. If n = m, the nanotubes are called ‘‘armchair”. If m = 0, the nanotubes are called ‘‘zigzag”. Otherwise, they are called ‘‘chiral”. An example of a chiral nanotube is shown in fig. 2.3[27, 28].

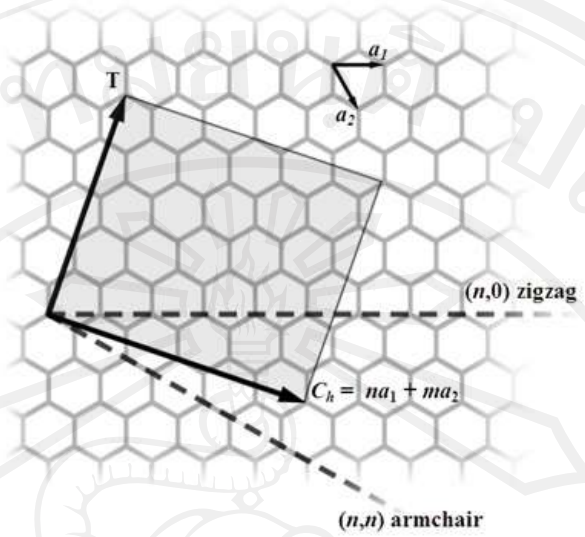

Figure 2.2 The graphite plane of nanotube surface coordinates [27]

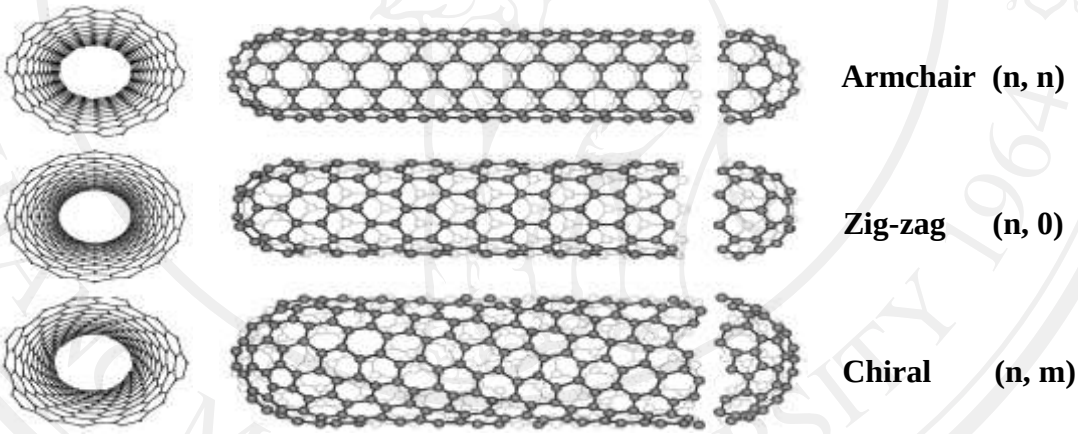

Figure 2.3 Structural of carbon Nanotube (a) Armchair structure (n, n), (b) zig-zag structure (n, 0), and (c) Chiral structure (n, m) [28]

2) Synthesis of carbon nanotubes (CNTs)

The arc-evaporation method, which produces the best quality nanotubes, involves passing a current of about 50 amps between two graphite electrodes in an atmosphere of helium. This causes the graphite to vaporize, some of it condensing on the walls of the reaction vessel and some of it on the cathode. It is the deposit on the

cathode which contains the carbon nanotubes. Single-walled nanotubes are produced when Co and Ni or some other metal is added to the anode. It has been known since the 1950s, if not earlier, that carbon nanotubes can also be made by passing a carbon containing gas, such as a hydrocarbon, over a catalyst. The catalyst consists of nanosized particles of metal, usually Fe, Co or Ni. These particles catalyze the breakdown of the gaseous molecules into carbon, and a tube then begins to grow with a metal particle at the tip. It was shown in 1996 that single-walled nanotubes can also be produced catalytically. The perfection of carbon nanotubes produced in this way has generally been poorer than those made by arc-evaporation, but great improvements in the technique have been made in recent years. The big advantage of catalytic synthesis over arc-evaporation is that it can be scaled up for volume production. The third important method for making carbon nanotubes involves using a powerful laser to vaporize a metal-graphite target. This can be used to produce single-walled tubes with high yield.

3) Properties of carbon nanotubes

The strength of the sp^2 carbon-carbon bonds gives carbon nanotubes excellent mechanical properties. The stiffness of a material is measured in terms of its Young's modulus, the rate of change of stress with applied strain. The Young's modulus of the best nanotubes can be as high as 1,000 GPa which is approximately 5x higher than steel. The tensile strength, or breaking strain of nanotubes can be up to 63 GPa, around 50x higher than steel. These properties, coupled with the lightness of carbon nanotubes, give them great potential in applications such as aerospace. The electronic properties of carbon nanotubes are also extraordinary. Especially notable is the fact

that nanotubes can be metallic or semiconducting depending on their structure. Thus, some nanotubes have conductivities higher than that of copper, while others behave more like silicon. There is great interest in the possibility of constructing nano-scale electronic devices from nanotubes, and some progress is being made in this area. However, in order to construct a useful device we would need to arrange many thousands of nanotubes in a defined pattern, and we do not yet have the degree of control necessary to achieve this. There are several areas of technology where carbon nanotubes are already being used. These include flat-panel displays, scanning probe microscopes and sensing devices. The unique properties of carbon nanotubes will undoubtedly lead to many more applications [26].

4) Applications of carbon nanotubes

Carbon nanotubes have extraordinary electrical conductivity, heat conductivity, and mechanical properties. They are probably the best electron field-emitter possible. They are polymers of pure carbon that can be reacted, and manipulated using the tremendously rich chemistry of carbon. This provides opportunity to modify the structure and to optimize solubility and dispersion. Very significantly, carbon nanotubes are molecularly perfect, which means that they are free of property-degrading flaws in the nanotube structure. Their material properties can therefore approach closely the very high levels intrinsic to them. These extraordinary characteristics give carbon nanotubes potential in numerous applications.

- **Field Emission** Carbon nanotubes are the best-known field emitters of any material. This is understandable, given their high electrical conductivity, and the unbeatable sharpness of their tip (the sharper the tip, the more concentrated will be an

electric field, leading to field emission; this is the same reason lightening rods are sharp). The sharpness of the tip also means that they emit at especially low voltage, an important fact for building electrical devices that utilize this feature. Carbon nanotubes can carry an astonishingly high current density, possibly as high as 1013 A/cm^2. Furthermore, the current is extremely stable. An immediate application of this behavior receiving considerable interest is in field-emission flat-panel displays. Instead of a single electron gun, as in a traditional cathode ray tube display, here there is a separate electron gun (or many) for each pixel in the display. The high current density, low turn-on and operating voltage, and steady, long-lived behavior make carbon nanotubes attract field emitters to enable this application. Other applications utilizing the field-emission characteristics of carbon nanotubes include general cold-cathode lighting sources, lightning arrestors, and electron microscope sources.

- **Conductive Plastics** Much of the history of plastics over the last half century has been as a replacement for metal. For structural applications, plastics have made tremendous headway, but not where electrical conductivity is required, plastics being famously good electrical insulators. This deficiency is overcome by loading plastics up with conductive fillers, such as carbon black and graphite fibers (the larger ones used to make golf clubs and tennis racquets). The loading required to provide the necessary conductivity is typically high, however, resulting in heavy parts, and more importantly, plastic parts whose structural properties are highly degraded. It is well established that the higher aspect ratio of filler, the lower loading required achieving a given level of conductivity. Carbon nanotubes are ideal in this sense, since they have the highest aspect ratio of any carbon fiber. In addition, their natural tendency to form ropes provides inherently very long conductive pathways even at ultra-low loadings.

Applications that exploit this behavior of carbon nanotubes include EMI/RFI shielding composites and coatings for enclosures, gaskets, and other uses; electrostatic dissipation (ESD), and antistatic materials and (even transparent!) coatings; and radar absorbing materials.

- **Energy Storage** Carbon nanotubes have the intrinsic characteristics desired in material used as electrodes in batteries and capacitors, two technologies of rapidly increasing importance. Carbon nanotubes have a tremendously high surface area (~1,000 m^2/g), good electrical conductivity, and very importantly, their linear geometry makes their surface highly accessible to the electrolyte. Research has shown that carbon nanotubes have the highest reversible capacity of any carbon material for use in lithium-ion batteries. In addition, carbon nanotubes are outstanding materials for super capacitor electrodes and are now being marketed. Carbon nanotubes also have applications in a variety of fuel cell components. They have a number of properties including high surface area and thermal conductivity that make them useful as electrode catalyst supports in PEM fuel cells. They may also be used in gas diffusion layers as well as current collectors because of their high electrical conductivity. Carbon nanotubes ' high strength and toughness to weight characteristics may also prove valuable as part of composite components in fuel cells that are deployed in transport applications where durability is extremely important.
- **Conductive Adhesives and Connectors** The same issues that make carbon nanotubes attractive as conductive fillers for use in shielding, ESD materials, etc., make them attractive for electronics materials, such as adhesives and other connectors (e.g., solders).

- **Molecular Electronics** The idea of building electronic circuits out of the essential building blocks of materials - molecules - has seen a revival the past five years, and it is a key component of nanotechnology. In any electronic circuit, but particularly as dimensions shrink to the nano-scale, the interconnections between switches and other active devices become increasingly important. Their geometry, electrical conductivity, and ability to be precisely derived, make carbon nanotubes the ideal candidates for the connections in molecular electronics. In addition, they have been demonstrated as switches themselves.

- **Thermal Materials** The record-setting anisotropic thermal conductivity of carbon nanotubes is enabling applications where heat needs to move from one place to another. Such an application is electronics, particularly advanced computing, where uncooled chips now routinely reach over 100°C. CNI's technology for creating aligned structures and ribbons of carbon nanotubes is a step toward realizing incredibly efficient heat conduits. In addition, composites with carbon nanotubes have been shown to dramatically increase the bulk thermal conductivity at small loadings.

- **Structural Composites** The world-record properties of carbon nanotubes are not limited to electrical and thermal conductivities, but also include mechanical properties, such as stiffness, toughness, and strength. These properties lead to a wealth of applications exploiting them, including advanced composites requiring high values in one or more of these properties.

- **Fibers and Fabrics** recently, fibers spun of pure carbon nanotubes have been demonstrated and they are undergoing rapid development, along with carbon nanotubes composite fibers. Such super strong fibers will have applications including body and vehicle armor, transmission line cables, woven fabrics and textiles.

- **Catalyst Supports** Carbon nanotubes have an intrinsically high surface area; in fact, every atom is not just on a surface - each atom is on two surfaces, the inside and outside. Combined with the ability to attach essentially any chemical species to their sidewalls provides an opportunity for unique catalyst supports. Their electrical conductivity may also be exploited in the search for new catalysts and catalytic behavior.

- **Biomedical Applications** The exploration of carbon nanotubes in biomedical applications is just underway, but has significant potential. Cells have been shown to grow on carbon nanotubes, so they appear to have no toxic effect. The cells also do not adhere to the carbon nanotubes, potentially giving rise to applications such as coatings for prosthetics and anti-fouling coatings for ships. The ability to chemically modify the sidewalls of carbon nanotubes also leads to biomedical applications such as vascular stents, and neuron growth and regeneration.

- **Other Applications** There is a wealth of other potential applications for carbon nanotubes, such as solar collection; nanoporous filters; catalyst supports; and coatings of all sorts. There are almost certainly many unanticipated applications for this remarkable material that will come to light in the years ahead and which may prove to be the most important and valuable of all [28].

2.3.2 Silicon carbide nanowires (SiCNWs)

Since the introduction of carbon nanotubes in 1992, the study of one-dimensional nanomaterials, which includes metallic, magnetic, semiconducting and oxide compounds has attracted considerable interest, especially as regards nanowires (NW), nanobelts and nanorods [29].

The main interests of this research are in the realization of nanoelectronic devices (e.g. nano field-effect transistors), nano-electromechanical systems, and nano-sensors exploiting high selectivity and compatibility with biological systems. Nanostructures may present very different characteristic and novel properties with respect to the corresponding bulk material, and they have important physical and chemical properties, in particular large specific surface/volume ratio and quantum size effects, which permit many applications such as nanoscale devices, sensors and scanning probes not possible with standard structures. [30]

1) Structure of SiCNWs

The crystalline structure of SiC can be considered to consist of the close-packed stacking of double layers of Si and C atoms. Each C (Si) is surrounded by four Si (C) atoms covalently bonded. The distance between neighboring Si and C atoms is approximately 3.08 Å for all polytypes. There are more than 200 polytypes in existence. The polytypes can be defined by the number of stacking order in a unit cell. The atom arrangements of popular polytypes are 3C, 4H, and 6H. The 3C-SiC polytype is the only cubic polytype and it has a stacking sequence ABCABC. 4H-SiC consists of an equal number of cubic and hexagonal bonds with stacking sequences of ABCB. Two-thirds of 6H-SiC is composed of cubic bonds and one-third of hexagonal bonds, with stacking sequences of ABCACB. Only 3C-SiC is referred to as β-SiC; other 4H- and 6H-SiC are called α-SiC. Fig. 2.4 shows the schematic diagram illustrating the stacking order of 2H-, 3C-, 4H-, and 6H-SiC. In general, β-SiC, which often appears at low temperature, is easy to nucleate and grow. However, 4H-SiC and

6H-SiC are known as high-temperature stable polytypes, which need relatively high temperatures to grow [31, 32].

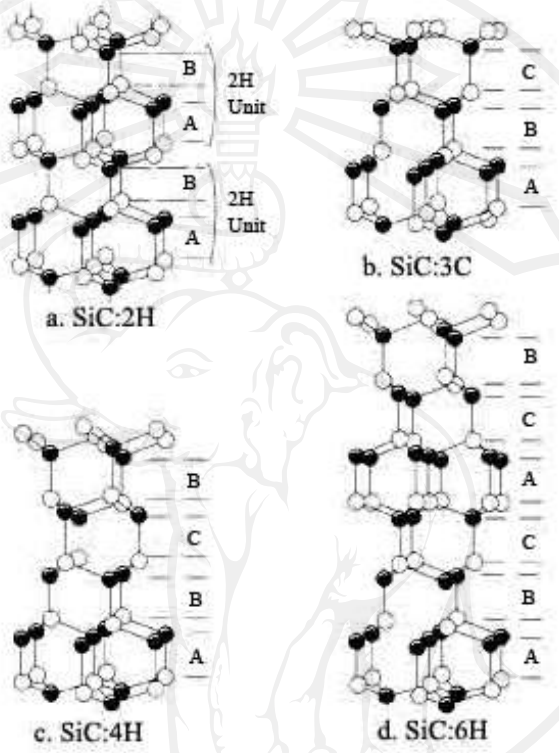

Figure 2.4 The stacking sequence of 2H-,3C-, 4H-, and 6H-SiC [32]

As it is known, silicon carbide crystallizes in many polytypes of so-called polymorphs in one measurement (their total amount is more than 200 [33]). For convenience of the further statement and comparison with nanosubjects, some characteristics of the most widespread polytypes are shown in table 2.1 and positions in the carbon and silicon atoms arrangement and structures are demonstrated in fig. 2.4. The SiC polytype content is defined by conditions of preparation (temperature, pressure, and environment) and presence of impurities. It is considered that cubic

polytype 3C-SiC is more stable in comparison with other hexagonal polytypes up to temperature of about 2,100 °C [31].

Table 2.1. The main physical and chemical properties of the most widespread SiC polytypes [33-34]

Properties	3C (β-SiC)	2H (α-SiC)	4H (α-SiC)	6H (α-SiC)
Space group	*F*43*m*	$P6_3mc$	$P6_3mc$	$P6_3mc$
Stacking order	*ABC*	*AB*	*ABCAB*	*ABCACB*
Hexagonality (%)	0	100	50	33
Lattice constant (nm)	a = 0.43596	a = 0.30753, c =0.50480	a = 0.30730, c = 1.0053	a =0.30806, c = 1.51173
Density (g/cm^3)	3.166	3.214	3.2	3.211
Melting point (°C)	2793	-	2830	2830
Thermal conductivity (W/cm/K)	3.6	-	3.7	4.9
Linear thermal expansion coefficient (10^5K)	3.9	-	-	4.46 a-axis 4.16 c-axis
Young's modulus (GPa)	~440	-	-	-
Mohs	9	9	9	9
Energy band gap (eV)	2.4		3.26	3.02

SiC materials are extremely hard, very inert, and have high thermal conductivity. Properties such as the breakdown electric field strength, the saturated

drift velocity, and the impurity ionization energies are unique for the different polytypes. β-SiC possesses the smallest band gap (~2.4eV) and has the highest electron carrier mobility compared with α-SiC, which makes it an important SiC material in the microelectronics industry [36]. Because of these excellent properties, SiC is a perfect material in the electronics industry, with a wide application in the areas of high-temperature device, high-power device, high-frequency device, and optoelectronic device, including rectifiers, power switches, RF, and microwave power devices [37, 38]. Besides, SiC, known for its high-temperature structure and reinforced composite material, can be also find application in the aerospace, car, machine, and petrochemical industries [38–44].

2) Synthesis of SiC Nanostructures

Since the discovery of the carbon nanotubes (CNTs) [44, 45], 1D SiC nanostructures have attracted many scientists because of their unique electronic, optical, and mechanical properties. A significant progress in synthesis methods in SiC nanowire/nanotube was achieved by various technologies, such as carbon template, arc discharge, chemical vapor deposition (CVD) via silicon precursor, carbothermal reduction of silica xerogels, etc. In this section, some recent progress in the fabrication of 1D SiC nanostructures is addressed [31].

- **Carbon Nanotubes-Confined Reaction**

In 1994, SiC whiskers were produced without the presence of metal catalysts by reacting carbon nanotubes with SiO at 1,700°C under a flow of Ar [46]. The length and diameter of the as-synthesized SiCNWs are one order greater in magnitude than that of the carbon nanotube precursor. The dark carbon nanotubes with hollow cores are

converted to solid greenish SiCNWs. The carbon nanotubes act as a template and define the diameter and length of SiC nanowires. The reaction is as follows:

$$2C(s) + SiO(g) \rightarrow SiC(s) + CO(g) \qquad (2.1)$$

In 1995, Lieber et al. [47] reported that carbon nanotubes could be converted to carbide rods by reaction with SiO or Si–I_2. The SiC nanorods are in high yield with typical diameters similar to or much smaller than the diameters of the carbon nanotubes, of between 2 and 30 nm and lengths of up to 20μm. A two-step reaction process has been developed to synthesize SiC nanorods at 1,400°C [48]. SiO vapor was generated via the silicon reduction of silica, and reacted with the carbon nanotubes to form SiC nanorods. In the two-step reaction process, the reaction equations are

$$SiO_2(s) + Si(s) \rightarrow 2SiO(v) \qquad (2.2)$$

$$SiO(v) + 2C(s) \rightarrow SiC(s) + CO(v) \qquad (2.3)$$

The nanorods are single-crystalline β-SiC with the diameters between 3 and 40 nm. The thinner SiC nanorods, namely 3 nm in diameter, show a high density of defect planes on the (111) basal planes. In this experiment, the diameter of the SiC nanowire differed from the precursor carbon nanotubes. It may be explained as follows. The generated CO vapor in (2.3) can react with SiO vapor on the generated SiC nanorod surface by the following reaction:

$$SiO(v) + 2CO(v) \rightarrow SiC(s) + CO_2(v) \qquad (2.4)$$

In this reaction, the diameter of the synthesized SiC nanorods is larger than that of the starting carbon nanotubes. On the contrary, the thinner diameters of SiC nanorods can be explained by the following reaction.

$$C(s) + CO_2(v) \rightarrow 2CO(v) \qquad (2.5)$$

The surface of the carbon nanotubes is consumed by the CO_2 and the residual carbon nanotube reaction with SiO leads to thinner SiC nanorods. The diameter and shape of the produced SiC nanorods can be controlled by the local partial pressure of CO gas and the reaction temperature, respectively. Tang et al. [49] developed a new way as shown in fig. 2.5.

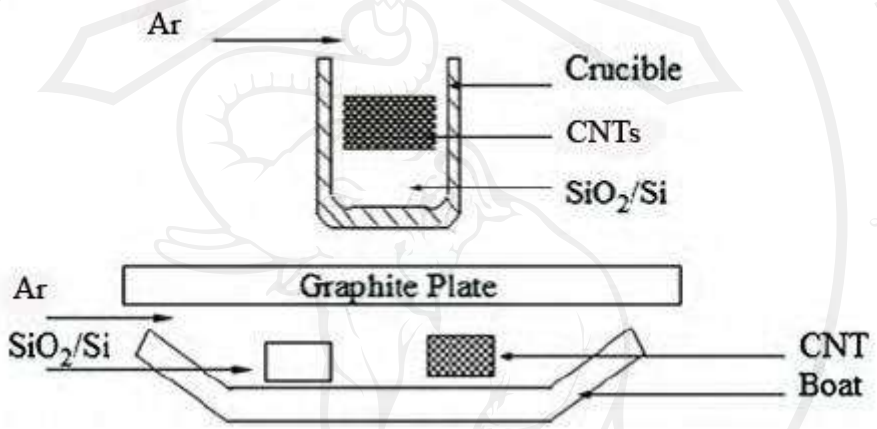

Figure 2.5 Geometry of the reactor. (a) Reactants of SiO_2/Si source covered with carbon nanotubes were put in a crucible. (b) SiO_2/Si source and carbon nanotubes were put in a boat and the latter kept clear of the former along the downstream direction of gas flowing [49]

The generated CO byproduct from (2.3) can be effectively carried away from the reaction area, thus preventing reactions (2.4) and (2.5). The size of the diameter of SiCNWs is consistent with the starting carbon nanotubes. The growth mechanism of SiC nanorods is basically a shape memory synthesis, where the product keeps the shape of the starting nanotubes to form nanorods. The shape memory synthesis has the advantages of the shape of the generated nanorods adjusted by the initial carbon nanotubes, the CO generated concentration, and reaction temperature. The unexpected

synthesis of SiC nanorods with thermally annealing single-walled carbon nanotube sheets (SWNTs) formed by a filtration process using surfactant- dispersed nanotubes, at a significantly lower temperature of 1,000°C between two silicon wafers [50]. In the experiment, the exterior layers of the carbon nanotube sheets were converted into a network of SiC nanorods, while the carbon nanotubes interior to the sheet remained unchanged. The SEM images are shown in fig. 2.6.

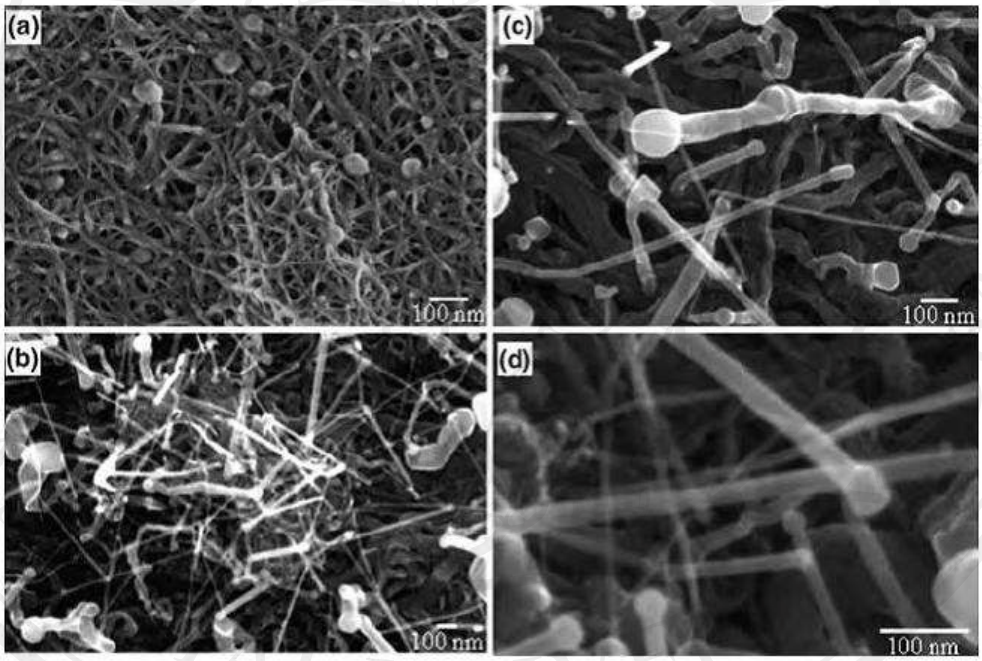

Figure 2.6 SEM micrographs of a carbon nanotube sheet before (a) and SiC nanorods: after (b)–(d) thermal annealing this sheet at 1,000°C between two parallel silicon wafers. The large quasi-spherical particles in (a), with a diameter of typically above 30 nm, contain iron [50]

- **Arc Discharge**

Since carbon nanotubes were synthesized by arc discharge, scientists attempted to fabricate SiCNWs with the arc-discharge process, considering the simple

setup, ease of operation and high production. Seeger et al. [51] synthesized of nanometer-sized SiC whiskers using the arc-discharge process. The samples were synthesized using an arc discharge between two graphite electrodes, the anode of which was filled with a mixture SiO_2 and C powder in the atomic ratio 1:1. The arc discharge was ignited by 40A at 22V under a 53 kPa helium atmosphere. The graphite cathode of 10mm diameter was placed horizontally, facing the composite anode of 6.15 mm diameter, which had a 3.2 mm diameter hole drilled, with 25mm filled with a mixture of graphite and Si powder. β-SiC whiskers of 10 nm in diameter were synthesized directly.

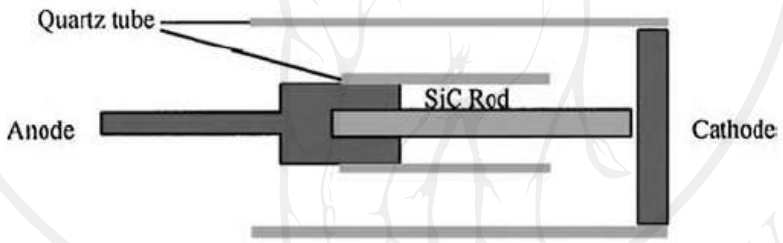

Figure 2.7 Arc-discharge setup [52]

Later, Li et al. [52] devised a new route, using a SiC rod as the anode in an arc-discharge process, developed to fabricate SiC nanorods on a large scale as shown in fig. 2.7. A graphite rod had a hole drilled at one end and its other end was thinned to 6mm in diameter. A SiC rod was inserted into the hole and acted as the anode, and a graphite plate was used as the cathode. The characterization indicated that the prepared nanorods possess a β-SiC crystal core with a uniform diameter of 5–20 nm and an amorphous SiO_2 wrapping layer tens of nanometers in thickness, and their lengths ranging from hundreds of nanometers to several micrometers is shown in fig.2.8. A possible growth mechanism could be explained as follows: during

discharging, SiC at the tip of the anode decomposes into silicon and carbon due to the high temperature of the arc-zone.

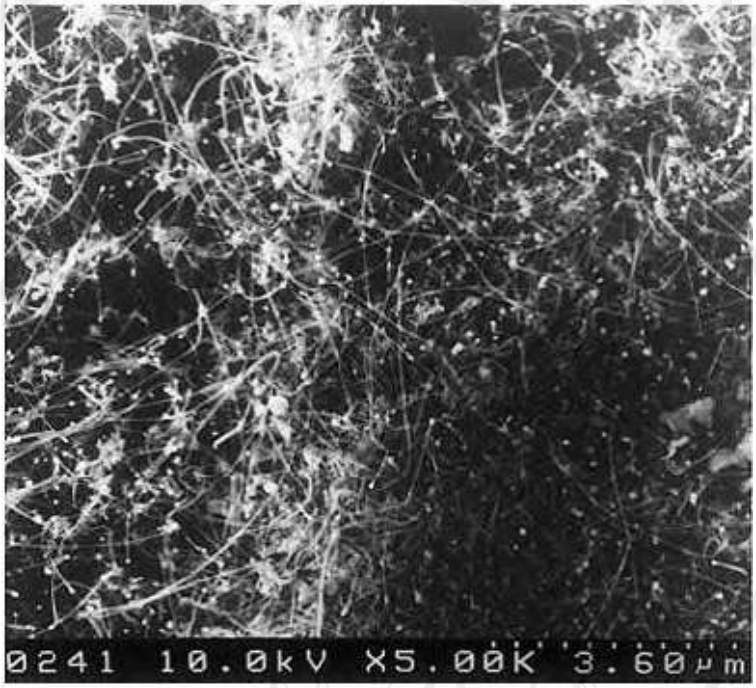

Figure 2.8 SEM image of the powder by arc discharge [52]

$$SiC(s) \rightarrow Si(g)+C(g) \qquad (2.6)$$

The silicon gas may react with the quartz (SiO_2) to form SiO gas.

$$SiO_2(s) + Si(g) \rightarrow 2SiO(g) \qquad (2.7)$$

Hence, the Si, C, and SiO gas were absorbed and dissolved in the liquid-iron droplets to form a liquid Fe–Si–C–O alloy. When cooled, the liquid droplets were supersaturated and the β-SiC core together with the SiO_2 sheath was nucleated.

- **Laser Ablation**

Laser ablation has been widely synthesized for carbon nanotubes [53, 54] and Si nanowires [55, 56], because the method can produce free-standing nanoscale material in high-purity yields at a low working temperature for high-melting and

multi-component materials. Shi et al. [57] used the laser-ablation technique to synthesized SiC nanowires from a target of SiC target (25x25x5mm) as shown in fig. 2.9. The KrF excimer pulsed laser beam was focused on the SiC target and the ablation lasted for 2 h. Large quantities of straight, curved, and randomly oriented nanowires were formed on the graphite substrate in the system. Fig. 2.10 shows the lengths of the nanowires were up to tens of micrometers.

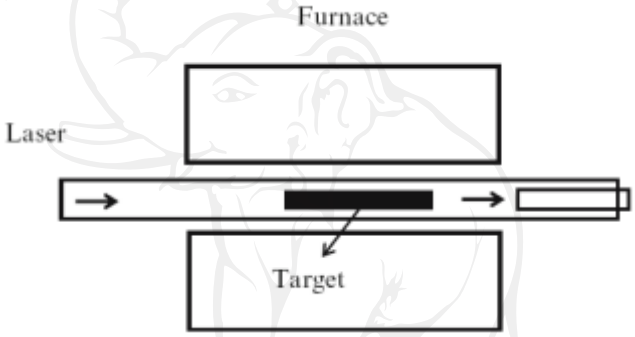

Figure 2.9 Laser-ablation scheme [57]

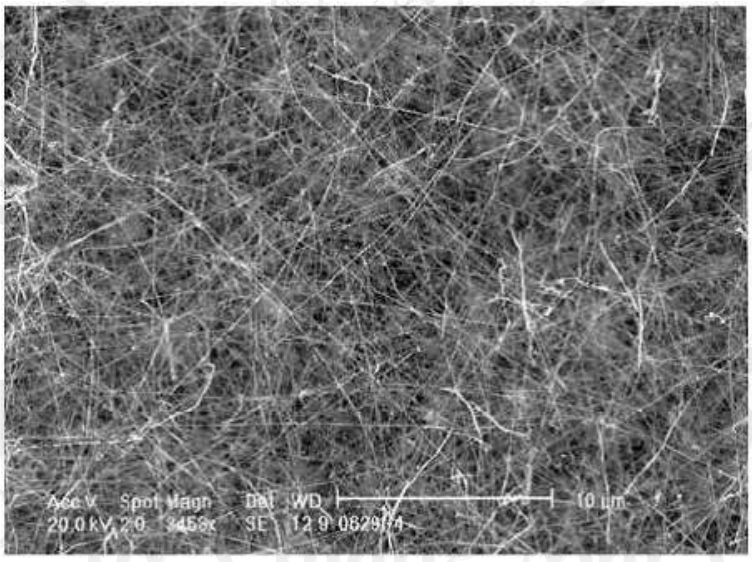

Figure 2.10 Typical SEM image of SiCNWs [57]

- **Sol-Gel and Carbothermal Reduction**

Meng et al. [58, 59] have successfully developed a novel method to synthesize bulk quantities of β-SiCNWs from silica xerogels containing carbon nanoparticles. The nanowires were fabricated by carbothermal reduction at 1,650°C for 1.5 h, followed by annealing to 1,800°C and holding for 30min in flowing Ar atmosphere. TEM, SAED, and EDX show the nanowires consist of 10–25 nm diameter crystalline β-SiC cores surrounded by amorphous SiO_2 sheathes with outer diameters between 20 and 70 nm. The nanowires formed by carbothermal reduction at 1,650°C for 2.5 h in flowing argon atmosphere are bare SiCNWs with diameters in the range of 15–30 nm.

Zu et al. [60] synthesized silicon carbide nanorods by sol-gel and carbothermal reduction processing with TEOS (tetraethoxysilane) and PVP (polyvinyl pyrrolidone) as starting materials and $Fe(NO_3)_3$ as catalyst. Results show the morphologies of the resulting sample are tower-like β-SiC nanorods which typically have a tower base width between 80 and 100 nm, a step layer thickness of about 10 nm between two layers and a height from 0.4 to 1.0μm as showed in fig. 2.11.

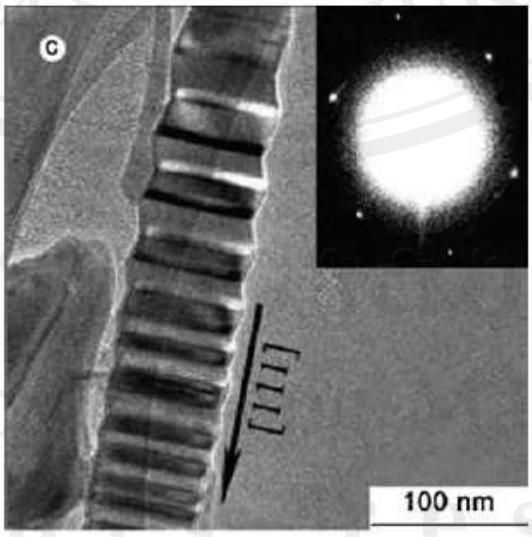

Figure 2.11 TEM images of resulting SiC sample catalyzed by Fe [60]

- **Chemical Vapor Deposition**

A mixture of silicon (carbon) precursor of SiH_4($SiCl_4$, $Si(CH_3)Cl$, CH_3SiCl_3,CH_4) is introduced into the reaction chamber [61–63]. During the reaction, SiCNWs are formed on the substrate by the reaction of carbon and silicon. Although this is at the cost of lower yield, the catalyst can be deposited on the desired location of substrate, which allows for the formation of novel nanostructures by predefined position of catalyst [64].

Zhang et al. [65] used microwave plasma CVD to synthesize bulk quantity singe crystalline β-SiCNWs on a Si substrate. The process is divided into two steps: first, smooth Si(100) substrates of 10x20x0.6mm were ultrasonically cleaned in ethanol and etched with 3% HF acid in water for 3 min. An Fe film of a different thickness (9–105 nm) was deposited on the Si(100) substrate by the sputtering method. Then the Si substrate was placed in the CVD system. A 100 sccm hydrogen (H_2) and a 0.05sccm methane (CH_4) were introduced into the chamber. The Si substrate temperature is from 800 to 1,000°C. Fig. 2.12 shows the TEM images of the as-synthesized SiCNWs by the CVD method. The SiCNWs are smooth and straight. Many nanowires are cylinder shaped with a circular cross section, while some of the nanowires have cross-sectional shapes of squares, rectangles, triangles, and hexagons. Moreover, no Fe catalyst has been found on the nanowires.

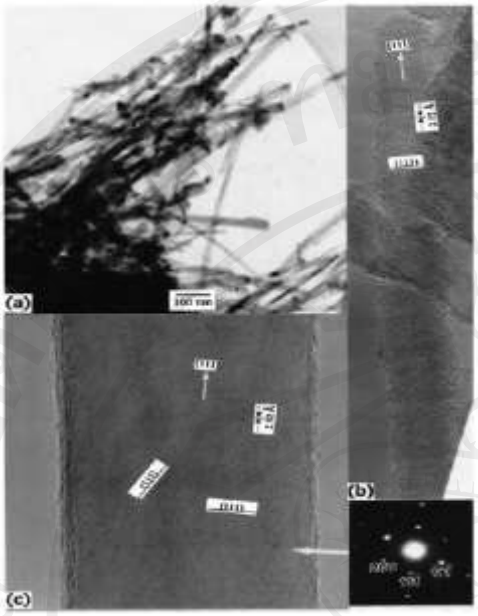

Figure 2.12 (a) TEM image of the nanowhiskers obtained by scratching the nanowhiskers from the Si substrate. (b) HR-TEM image of a thin 3C-SiC nanowhisker with an orientation of [111]. (c) A thick 3C-SiC nanowhisker with its selected area electron diffraction pattern taken by the electron beam parallel to the [011] zone axis [65]

Zhou et al. [66] synthesized SiC nanorods on silicon substrate by hot filament CVD. The carbon and silicon powders in a molar ratio of 1:1 were mixed and pressed into a solid disk and loaded into a HFCVD chamber. Hydrogen fed into the chamber etched the Si/C solid disk and brought Si/C-containing reactive species to the substrate surface. After 2 h, nanowires of SiC with a 10–30 nm diameter core– shell structure were found deposited directly on the substrate surface SiCNWs with diameters of about 50 nm and lengths of several micrometers have been fabricated on Si substrates coated with a thickness of 2 nm Ni film by direct current magnetron sputtering methods

Chio et.al [67] used methyltrichlorosilane (MTS, CH_3SiCl_3) as a source precursor because it has an equivalent ratio of Si to C and decomposes at a low temperature. H_2 was used both as the carrier gas, which are transfers the source precursor through a bubbler to the quartz reactor, and as a diluent gas, which regulates the concentration of the mixture containing MTS vapor and carrier gas. The XRD,

TEM, and HRTEM observations confirm that the nanowires are single-crystalline cubic structures with a [111] direction and SiCNW growth via the VLS mechanism. Fig. 2.13 shows that the SiCNWs grow under a reactor pressure of ca. 5 Torr for 2 h. The nanowires have diameters from several tens to hundreds of nanometers and are vertically well aligned without templates such as anodic alumina templates.

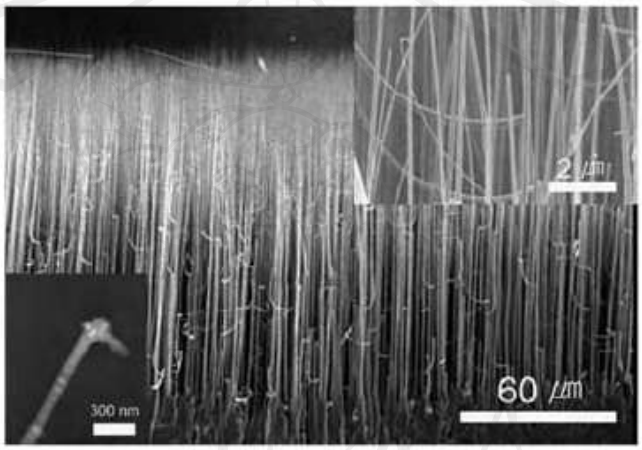

Figure 2.13 SEM images of vertically aligned SiCNWs grown on a Si substrate at 1,100°C for 2h under total reactor pressure of 5 Torr. The hydrogen flow rate at 775cm^3 min^{-1}. *Left lower inset* is a TEM image of SiCNWs [67]

Li et al. [68] synthesized semiconductor SiC nanonetworks at relatively low temperature (1,250°C) via CVD method. The mixture of Si and SiO_2 powders and C_3H_6 were used as precursor materials. The straight or curved SiC networks that the nanowires are connected to were formed on carbon cloth. The nanowires with diameter of about 20–70 nm are single-crystalline β-SiC and the growth direction is along [111].

Zhang et al. [69] synthesized SiC nanorods by floating catalyst methods. Iron particle catalyst was decomposed from ferrocene vapor while being carried into the

chamber by the flowing gases. In the $SiCl_4$–C_6H_6–H_2–Ar system, $SiCl_4$ and C_6H_6 reacted with each other, catalyzed by the Fe cluster.

- **High-Frequency Induction Heating**

Zhou et al. [70] invented a novel method to fabricate β-SiCNWs without catalyst introduction in high yield on the surface of the activated carbon fibers (ACFs). The experiments were performed in a vertically set high-frequency induction-heating furnace as schematically outlined in fig. 2.14, which is consisted of a quartz tube and an inductive heat cylinder of graphite coated by a layer of ACFs. Firstly, 2 g of commercial SiO powder (99.9%) was put into a graphite crucible. Before heating, the chamber was flushed with high-purity 100 sccm Ar to eliminate O_2 by means of rotary vacuum pump for three times. Afterwards, the furnace was rapidly heated from room temperature to around 1,450°C within 2 min and maintained for reaction for 15 min under a total pressure of 50–100 Torr. After the furnace was cooled to room temperature in the flowing Ar, the ACFs surface was deposited with a thick layer of light-blue fluff-like products having a thickness of several millimeters as shown in the inset of fig. 2.15. Many mushroom-like lumps grew perpendicularly and separately from the surface of the ACF and joined each other at their tip.

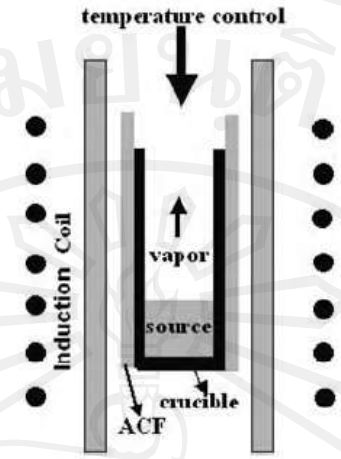

Figure 2.14 High-frequency induction-heating furnace [70]

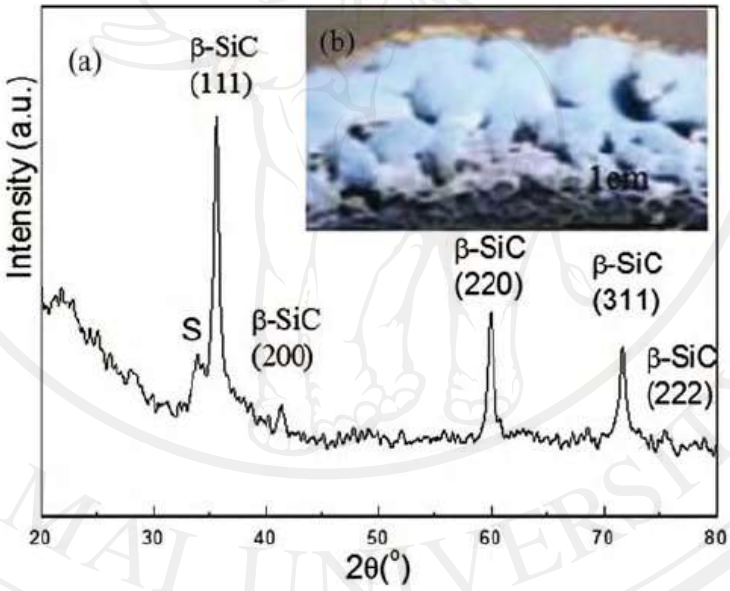

Figure 2.15 (a) XRD pattern of the as-synthesized products. *Inset* (b): the digital camera photo of the products [70]

The X-ray diffraction (XRD) pattern in fig. 2.15 suggests that the as-synthesized product consists of the crystalline zinc-blend (cubic) form of β-SiC with the unit constant of a = 4.358 °*A*, close to the standard value for β-SiC (4.359 A° , JCPDS card no. 29-1129). A broad peak at 2θ =~20°–30° may be attributed to some

amorphous materials with the product. Besides, there is a low-intensity peak (marked with S) at a lower diffraction angle than that of the strong (111) peak, which usually ascribes to the stacking faults in the (111) plane. The low-magnification SEM image shows in fig. 2.16a reveals that the product consists of numerous wire-like nanostructures (a large amount of straight, curved, randomly oriented, and free-standing nanowires) with a length of up to tens of micron. Fig. 2.16b shows the chemical composition of the nanowires characterized by EDS. It is found that the nanowires are mainly composed of Si, C, and O.

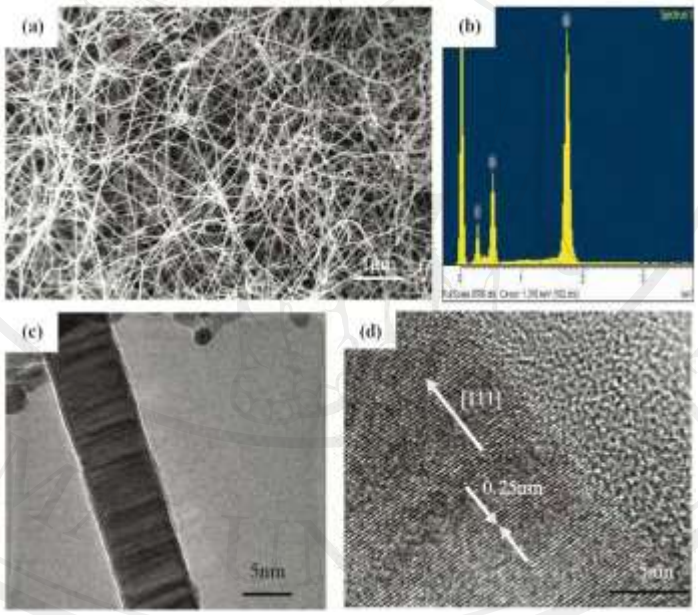

Figure 2.16 (a) SEM image of as-prepared samples grown at 1,450°C for 20 min by SiO powder and carbon fiber, (b) EDS spectrum of the nanowires, (c) TEM image of SiCNW, and (d) HRTEM image of the individual SiCNW [70]

The large resolution TEM image shows that a d-spacing of 0.25 nm corresponds to the (111) plane spacing, indicating that SiCNW grows along [111] direction.

In addition, Kong et al. [71] synthesized the SiC/SiO_2 nanosprings, as shown in fig. 2.17. The diameter of the nanospring is about 25nm and with the nanospring pitch of 10 nm, this amounts to a diameter/pitch ratio of 2.5. The total nanostructures consist of three segments: two end of the nanostructure is SiC/SiO_2 nanocables, but SiC/SiO_2 nanospring is clearly seen in the midst of the whole nanostructure. TEM dark images (fig. 2.17b) indicate that the nanospring is composed of a crystalline core and an amorphous coating.

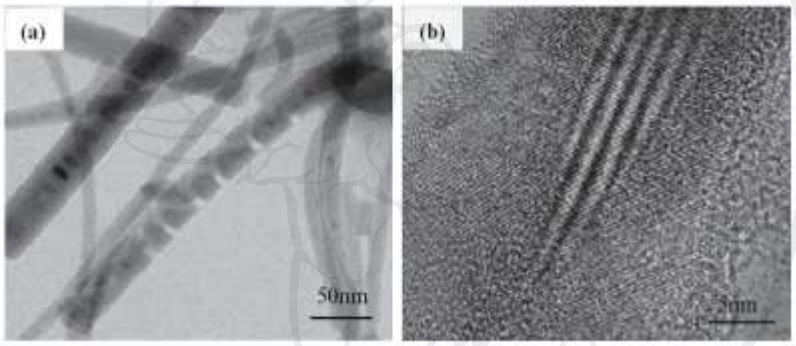

Figure 2.17 (a) Typical TEM images for SiC/SiO_2 nanosprings and (b) HRTEM image nanostructures [71]

- **The Current Heating**

Jintakosol and Singjai [71] used current heating to synthesize β-SiCNWs by mixing of C+ SiO_2 doped with Al_2O_3 powders in the rod shape. The rod was heated up to 1,400°C for 30 min. The as-grown nanowires have been successfully synthesized from the inner core. Observes found that the nanowires have diameters of ~50–200 nm and several microns in the length. Moreover, TEM images indicated that the NW was single-crystalline cubic structure with a [111] growth direction [72].

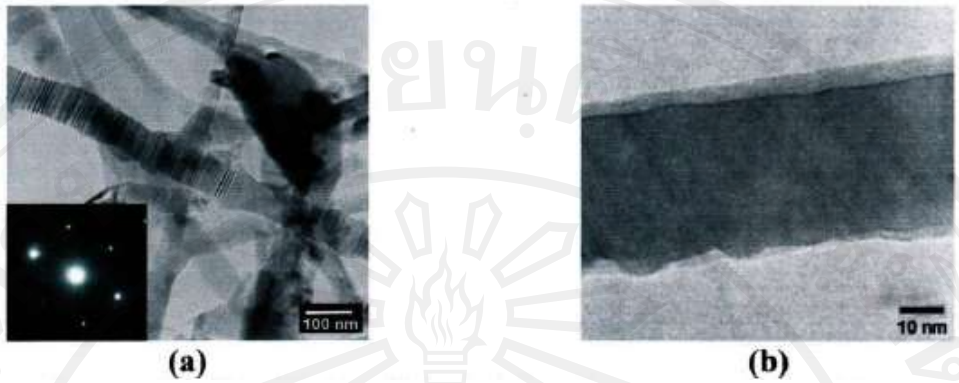

Figure 2.18 TEM images of (a) SiCNWs (1 wt.% doping); inset is a corresponding SAED pattern, shows a single-crystalline cubic structure with a [111] growth direction and (b) a non-uniform layer thickness of alumina coating on an individual SiCNWs (2 wt% doping) [72]

3.) Properties of SiCNWs

- **Field Emission**

Because of the small curvature of the tip radius, high ratio, chemical inertness, and electrical conductivity, SiC wide-band gap semiconductors are considered to be promising for the next generation of large-area filed-emission flat panel displays (FEDs) [73–77]. Zhou et al. [78] investigated the field-emission characteristics of the 1D SiC nanostructures, which indicate that the SiCNWs are characteristic of excellent emitting behavior for application in field-emission technology. In addition, a stability and durability test was carried out on the SiCNWs at anode-sample 100μm separation. Figure 2.19 shows the field-emission current density (J) of the SiCNWs as a function of the applied electric field (E) at three anode-sample separation: 100, 120, and 140μm. The turn-on field was defined as the electric field required producing a current density of 10μA cm^{-2}. It can be seen that the turn-on field is dependent on the anode-sample distance, its value increase as the anode-sample distances decrease, and

measured to be 3.5, 3.4, and 3.1Vμm^{-1}, respectively, which indicates the strong electron emission property of the SiCNWs because of the high aspect ratio and high specific surface area.

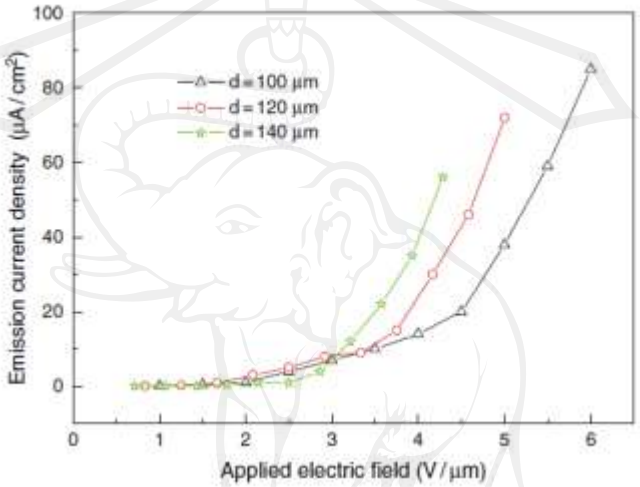

Figure 2.19 The dependence of the field-emission current density J on the applied electric field strength E of the samples at three anode-sample distances of 100, 120, and 140μm [78]

- **Optical Properties**

There have been some reports on the optical properties of SiCNWs. Experiments show that SiCNWs have a significant redshift owing to the size confinement effect. Fig. 2.20 shows the typical Raman spectra of SiCNWs and SiC bulk ceramic target [56]. The SiCNWs have the typical Raman features at about 784 and 938cm^{-1} and both peaks have a marked redshift of 12 and 34 cm^{-1} compared to the TO and LO phonon modes of bulk SiC.

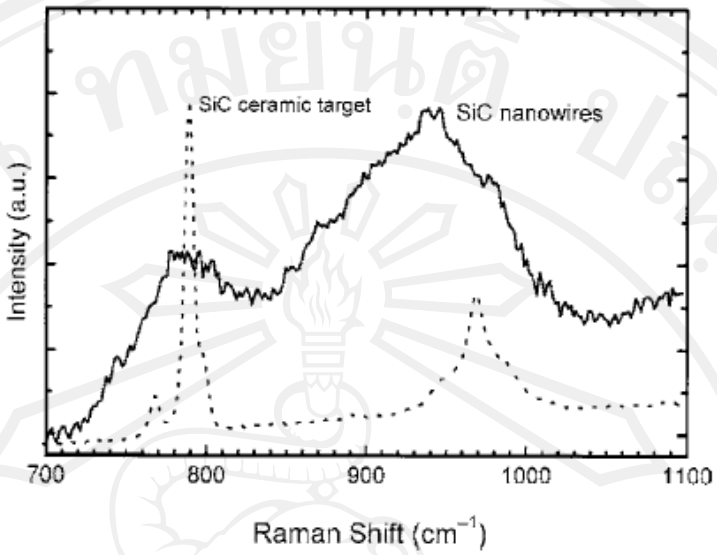

Figure 2.20 Raman spectrum of SiCNWs by laser ablation [56]

Liu et al. [79] synthesized SiC/SiO_2 nanocables by the low-cost arc-discharge method in deionized water. The SiC with 10 nm core diameters possesses two broad PL peaks at 317 and 368 nm as shown in fig. 2.21a. However, two emission peaks of the SiCNWs with 20 nm diameter are located at 312 and 393 nm. It is believed that the second peak results from the central β-SiCNW and the blue shift may be the result of the quantum size effects.

The PL spectra of the SiC with core diameter of 20 nm are shown in fig. 2.21b. It can be seen that the positions of the PL peaks slightly shift while the strength significantly changed. It can also be noted that high-temperature annealing would release the local stress formed during the growth of the nanocables and decrease the amount of defects; then the intensity of PL peak and position would change.

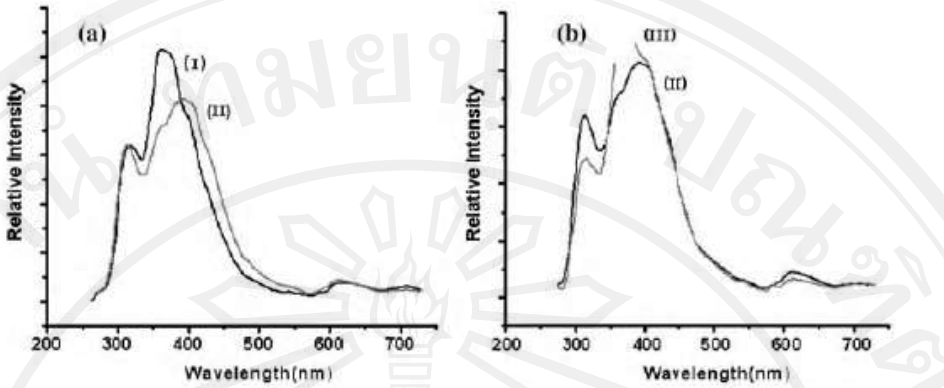

Figure 2.21 (a) PL spectra of the as-prepared SiC nanocables with core diameters of 10 nm (I) and 20 nm (II), respectively. (b) The PL spectra of the SiC nanocables with core diameter of 20 nm before (II) and after (III) annealing [79]

- **Mechanical Properties**

1D nanostructures are supposed to be significantly stronger than their counterparts. Wong et al [81] used atomic force microscopy to determine the mechanical properties of individual, structurally isolated SiC nanorods that were pinned at one end to molybdenum disulfide surfaces. The bending force was measured against displacement along the unpinned lengths. The strengths of the SiC nanorods were substantially greater (610–660 GPa) than those found previously for larger SiC structures, and they approach theoretical values. These results are in good agreement with the 600 GPa value predicted theoretically for [111] oriented SiC, the average values obtained previously for micrometer diameter whiskers.

Yang et al. [81-83] reported fabrication and flexural properties (measured by three-point bending) of a SiC nanowire/Tyranno-SA fiber-reinforced SiC/SiC composite made by the chemical vapor infiltration (CVI) process. A representative flexural stress–displacement curve is shown in fig. 2.22. The composite T-NFRC (T

stands for Tyranno-SA fiber and NFRC stands for SiC nanowire/fiber-reinforced composites) possesses common features with conventional Tyranno-SA/SiC composites upon flexural fracture. The measured values of SiCNW/fiber-reinforced composites suggest that SiCNWs can be used as reinforcement materials for ceramic matrix composites to improve their strength and toughness.

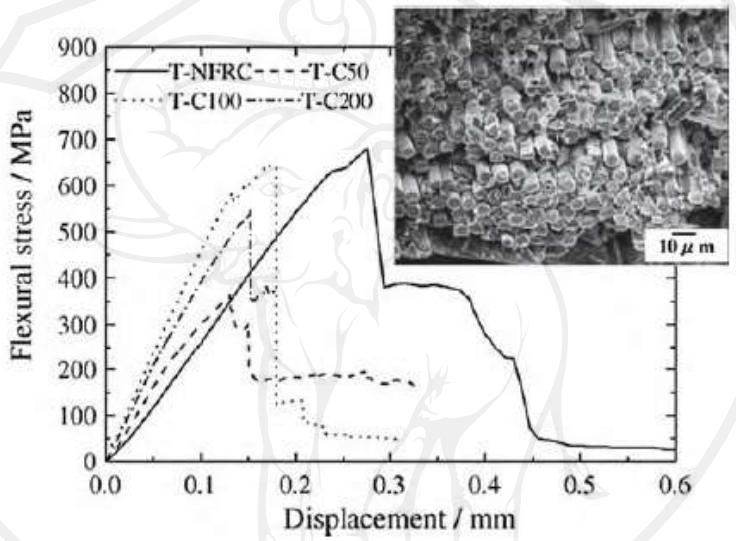

Figure 2.22 Typical flexural stress–displacement curves and fiber pullout fracture surface (T-NFRC) [81]

However, the SiCNW-reinforced Tyranno-SA/SiC composites show marked improvements on the flexural strength and work of fracture compared with a series of conventional Tyranno-SA/SiC composites (T-C50, T-C100, and T-C200). The flexural properties, such as flexural modulus (E_f), proportional limit stress (PLS), ultimate flexural strength (σ_u), and the fracture energies (W_f), are given in table 2.2.

Table 2.2 Density, interlayer, and flexural properties of composite with SiC nanowires and conventional composites [81]

Composite ID	Density ($Mg\ m^{-3}$)	Pyc layer (nm)	E_f (GPa)	PLS (MPa)	σ_u	W_f
T-NFRC	2.62±0.03	60	120±17	570±120	660±77	6.1±0.7
T-C50	2.41±0.03	50	140±13	260±5	410±92	1.8±0.5
T-C100	2.63±0.04	100	160±11	430±32	610±28	3.2±0.4
T-C200	2.61±0.03	200	140±10	340±18	550±58	2.3±0.3

Rao et al. [84] have investigated the mechanical properties of composites of SiC nanowire-reinforced polymer–matrix (PVA) composites. Experimental results show that enhancements of these mechanical properties occur even with a small vol% addition of SiCNWs. A representative curve of tensile stress vs. strain is shown in fig. 2.23. With increasing SiC nanowire volume fraction (V_f), a significant increase in the yield strength takes place. PVA without SiCNW reinforcement behaves like an elastic, perfectly plastic solid. The 0.8 vol% SiCNW composites show near zero ductility, fracturing immediately after yielding. The composites exhibit higher strength; a significant strain softening is seen immediately after the peak in the load.

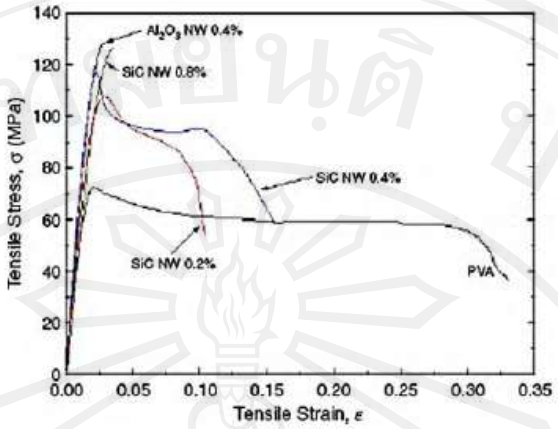

Figure 2.23 Tensile stress–strain curves of PVA and NW composites, shows an increase in the ultimate tensile strength and reduction in ductility with increasing NW volume fraction [84]

Fig. 2.24 shows tensile strength as a function of nanowire volume fraction. As for the SiC nanowire-reinforced composite, the strength of the composites increases markedly initially and reaches a plateau. The initial hardening rate is commensurate with the strength of the SiCNWs. The measured result is compatible with the least square fit of the equation.

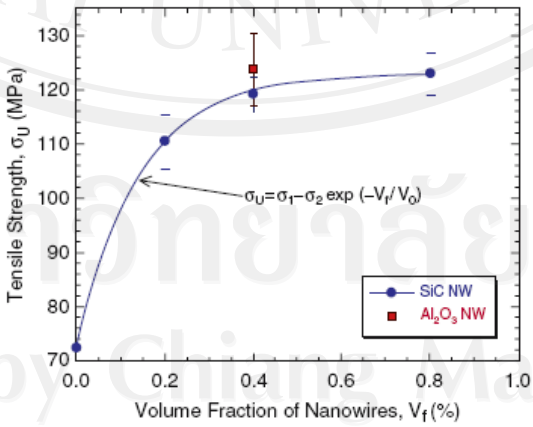

Figure 2.24 Variation of tensile strength as function of nanowire volume fraction. The *solid line* represents the least-square fit to the equation given in the figure [84]

- **Photocatalyst Properties**

Zhou et al. [85] evaluated the photocatalytic activity of the SiC nanowires by measuring the photodegradation rates of CH_3CHO for SiC in a quartz vessel as a function of UV irradiation time under UV light. From fig. 2.25a, it was found that the increase of the initial gaseous acetaldehyde concentration leads to a strengthened conversion of gaseous acetaldehyde. This is attributed to the larger amount of gaseous acetaldehyde molecules attached to the surface of the SiCNW powders. These results are also corroborated by the concentration variation of produced CO_2, evolved as result of photodecomposition of acetaldehyde, as a function of irradiation time. The CO_2 concentration increases with the photodegradation rate of gaseous acetaldehyde. That is to say, the acetaldehyde is converted into CO_2. Besides, the synthesized SiC NWs coated with SiO_2 layers have higher photocatalytic activity than the HF-treated (bare) SiCNWs.

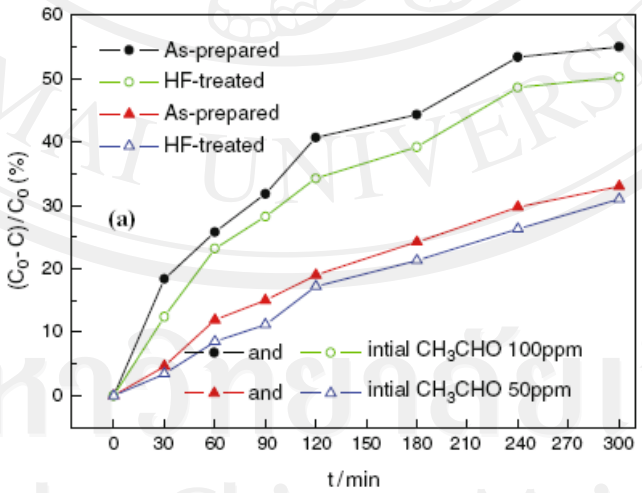

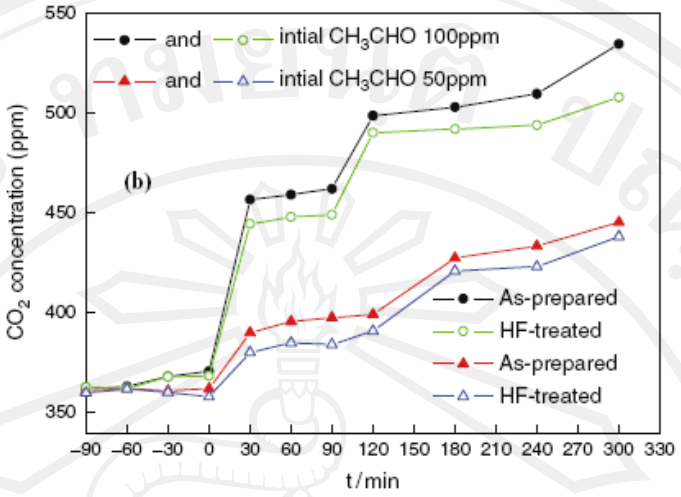

Figure 2.25 (a) SiC photodegradation rates as a function of irradiation time during the photodegradation of acetaldehyde gas under UV irradiation (C_0, C are initial, final concentration respectively) and (b) CO_2 evolution as a function of irradiation time (light on at zero) during the photodegradation of acetaldehyde gas under UV irradiation [85]

- **Hydrogen Storage Properties**

Recently, Mpourmpakis and Froudakis [86] reported hydrogen storage in SiCNTs by a multiscale theoretical approach. First, ab initio calculations at the density functional level of theory (DFT) showed an increase of 20% in the binding energy of H_2 in SiCNTs compared with pure CNTs. Second, classical Monte Carlo simulation of nanotube bundles showed an even larger increase of the storage capacity in SiCNTs, especially in low-temperature and high-pressure conditions. Both the results indicate that SiCNTs seem to be more suitable materials for hydrogen storage than pure CNTs.

4) Nanowires Growth techniques

An important aspect of the 1D structures relates to their crystallization [6], wherein the evolution of a solid from a vapor, a liquid, or a solid phase involves nucleation and growth. As the concentration of the building units (atoms, ions, or molecules) of a solid becomes sufficiently high, they aggregate into small nuclei or clusters through homogeneous nucleation. These clusters serve as seeds for further growth to form larger clusters. Several synthetic strategies have been developed for 1D nanowires with different levels of control over the growth parameters. These include:

a) the use of the anisotropic crystallographic structure of the solid to facilitate 1D nanowire growth
b) the introduction of a solid–liquid interface
c) use of templates (with 1D morphologies) to direct the formation of nanowires
d) supersaturation control to modify the growth habit of a seed
e) use of capping agents to kinetically control the growth rates of the various facets of a seed
f) self-assembly of zero-dimensional (0D) nanostructures.

They are conveniently categorized into growth in the vapor phase; and solution-based growth. [87]

In this section, focus on vapor phase growth, which is extensively used for producing nanowires. Starting with the simple evaporation technique in an appropriate atmosphere to produce elemental or oxide nanowires, vapor–liquid–solid, vapor–solid and other processes are also made use of:

4.1) Carbothermal reactions

Nanowires of a variety of oxides, nitrides and carbides can be synthesized by carbothermal reactions. Carbon (activated carbon or carbon nanotubes) in mixture with an oxide produces sub-oxidic vapor species which reacts with C, O_2, N_2 or NH_3 to produce the desired nanowires. For example, synthesis of Si_3N_4, carbothermal reactions generally involve the following steps:

$$SiO_2 + C \rightarrow SiO + CO \quad (2.6)$$

$$SiO + C \rightarrow Si + CO \quad (2.7)$$

$$3Si + 2N_2 \rightarrow Si_3N_4 \quad (2.8)$$

$$3SiO + 6C + 2N_2 \rightarrow Si_3N_4 + 6CO \quad (2.9)$$

The first step normally involves the formation of a metal sub-oxide by the reaction of the metal oxide with carbon. Depending on the desired product, the sub-oxide heated in the presence of O_2, NH_3, N_2 or C yields oxide, nitride or carbide nanowires [87].

4.2) Vapor–solid growth

It is possible to realize NW without a metal catalyst on the substrate surface, by thermal evaporation of a suitable source near its melting point and subsequent deposition at cooler temperature. This mechanism is called “vapor-solid” (VS) growth and has been mainly used to synthesize metal oxide and some semiconductor nanomaterials [88]. It is often called self-catalytic growth, since in this case one component of the gaseous atoms might play the role of the catalyst.

The VS method for whisker growth also holds for the growth of 1D nanomaterials [89]. In this process, evaporation, chemical reduction or gaseous reaction first generates the vapor. The vapor is subsequently transported and condensed onto a substrate. The VS method has been used to prepare whiskers of

oxide, as well as metals with micrometer diameters. Therefore, it is possible to synthesize the 1D nanostructures using the VS process if one can control the nucleation and the subsequent growth process. Using the VS method, nanowires of the oxides of Zn, Sn, In, Cd, Mg, Ga and Al have been obtained.

4.3) Oxide-assisted growth

Lee et al. [90, 91] proposed a nanowire growth mechanism called the oxide-assisted growth mechanism. No metal catalyst is required for the synthesis of nanowires by this means. Based on their experimental observations, these workers find that the growth of Si nanowires is greatly enhanced when SiO_2-containing Si powder targets were used. Limited quantities of Si nanowires were obtained even with a target made of pure Si powder.

Lee et al. [90] propose that the growth of the Si nanowires is assisted by the Si oxide, where the Si_xO ($x > 1$) vapor generated by thermal evaporation or laser ablation plays the key role. Nucleation of the nanoparticles is assumed to occur on the substrate. These decompositions result in the precipitation of Si nanoparticles, which act as the nuclei of the silicon nanowires covered by shells of silicon oxide. The precipitation, nucleation and growth of the nanowires occur in the area near the cold finger, suggesting that the temperature gradient provides the external driving force for the formation and growth of the nanowires.

Fig. 2.26 shows the TEM images of the formation of nanowire nuclei at the initial stages. Fig. 2.26a shows Si nanoparticles covered by an amorphous silicon oxide layer. The nanoparticles that are isolated with the growth directions and the substrate surface exhibit the fastest growth. Fig.2.27 shows a schematic of the nanowire growth by this mechanism. The growth of the silicon nanowires is

determined by four factors: (1) catalytic effect of the Si_xO ($x > 1$) layer on the nanowire tips; (2) retardation of the lateral growth of nanowires by the SiO_2 component in the shells, formed by the decomposition of SiO; (3) stacking faults along the nanowire growth direction of [112], and (4) the {111} surfaces, which have the lowest surface among the Si surfaces, playing an important role in nucleation and growth, since the energy of the system is reduced significantly when the {111} surfaces are parallel to the axis of the nanowires. The last two factors ensure that only the nuclei that have their [112] direction parallel to the growth direction grows fast (Fig.2.27b).

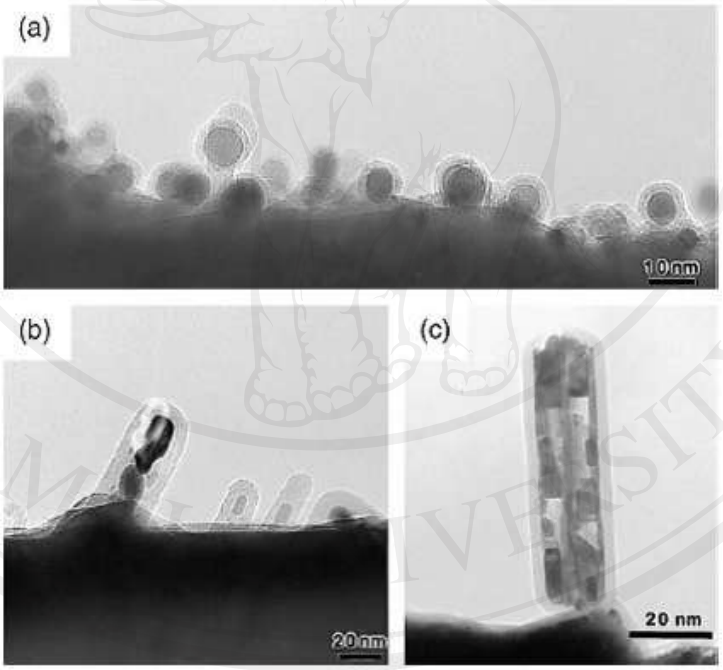

Figure 2.26 TEM micrographs of (a) Si nanowire nuclei formed on the Mo grid and (b), (c) initial growth stages of the nanowires [90]

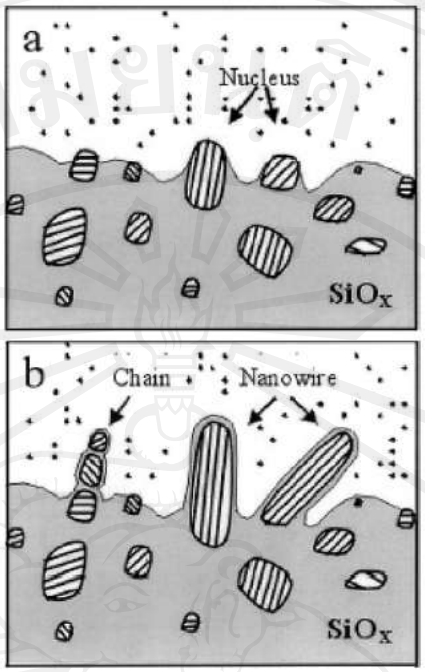

Figure 2.27 Schematic describing the nucleation and growth mechanism of SiNWs. The parallel lines indicate the [112] orientation. (a) Si oxide vapor is deposited first and forms the matrix within which the Si nanoparticles are precipitated. (b) Nanoparticles in a preferred orientation grow fast and form nanowires. Nanoparticles with non-preferred orientations may form chains of nanoparticles [90]

4.4) Vapor-liquid-solid method

The vapor-liquid-solid method (VLS) is a mechanism for the growth of one-dimensional structures, such as nanowires, from chemical vapor deposition. Growth of a crystal through direct adsorption of a gas phase on to a solid surface is generally very slow. The VLS mechanism circumvents this by introducing a catalytic liquid alloy phase which can rapidly adsorb a vapor to supersaturation levels, and from which crystal growth can subsequently occur from nucleated seeds at the liquid-solid interface. The physical characteristics of nanowires grown in this manner depend on the size and physical properties of the liquid alloy [92].

Wagner and Ellis [93] proposed the VLS mechanism by explanation for silicon whisker growth from the gas phase in the presence of a liquid gold droplet placed upon a silicon substrate. The explanation was motivated by the absence of axial screw dislocations in the whiskers, the requirement of the gold droplet for growth, and the presence of the droplet at the tip of the whisker during the entire growth process.

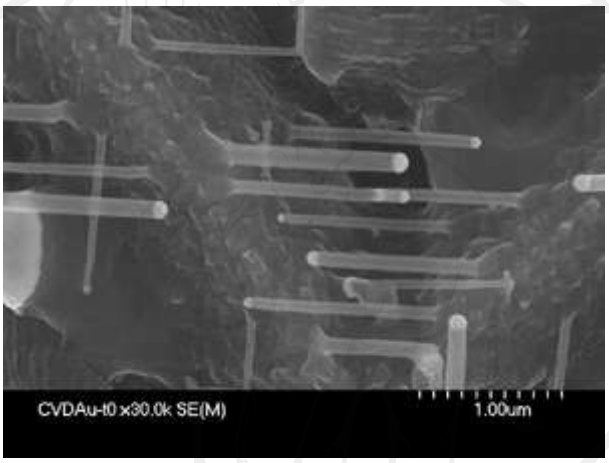

Figure 2.28 CVD Growth of Si nanowires using Au particle catalysts [93]

4.4.1) Requirements for catalyst particles

The requirements for catalyst are [92]:

- It must form a liquid solution with the crystalline material to be grown at the nanowire growth temperature.
- The solid solubility of the catalyzing agent is low in the solid and liquid phases of the substrate material.
- The equilibrium vapor pressure of the catalyst over the liquid alloy be small so that the droplet does not vaporize, then shrink in volume and decrease the radius of the growing wire until growth is terminated.

- The catalyst must be inert (non-reacting) to the reaction products (during CVD nanowire growth).
- The vapor-solid, vapor-liquid, and liquid-solid interfacial energies play a key role in the shape of the droplets and therefore must be examined before choosing a suitable catalyst; small contact angle between the droplet and solid are more suitable for large area growth while large contacts angles result in smaller (decreased radius) whisker formations.
- The solid-liquid interface must be well defined crystallographically in order to produce highly directional growth of nanowires. It is also important to point out that the solid-liquid interface cannot be completely smooth. Furthermore, if the solid liquid interface was atomically smooth, atoms near the interface trying to attach to the solid would have no place to attach to until a new island nucleates (atoms attach at step ledges), leading to an extremely long growth rate. Therefore, "rough" solid surfaces, or surfaces containing a large number of surface atomic steps (ideally 1 atom wide, for large growth rates) are needed for depositing atoms to attach and nanowire growth to proceed.

4.4.2) Growth mechanism

Wu and Yang [94] reported real-time observations of Ge nanowire growth in an in situ high-temperature TEM, which demonstrate the validity of the VLS growth mechanism. The growth of Ge nanowires using Au clusters as a solvent at high temperature is explained based on the Ge-Au phase diagram shown in fig. 2.30. Ge and Au form a liquid alloy when the temperature is higher than the eutectic point (363 °C) as shown in fig. 2.20a-I. The liquid surface has a large accommodation coefficient and is therefore a preferred deposition site for the incoming Ge vapor. After the liquid alloy becomes supersaturated with Ge, precipitation of the Ge nanowire occurs at the

solid-liquid interface (fig. 2.30a II-III). Their experimental observations suggest that there are three growth stages: metal alloying, crystal nucleation and axial growth as shown in fig. 2.29 which shows a sequence of TEM images during the in situ growth of a Ge nanowire. Three stages are clearly identified.

a) Alloying process as shown in fig. 2.29a–c: The maximum temperature that could be attained in the system was 900 °C, up to which the Au clusters remain in the solid state in the absence of Ge vapor. With increasing amount of Ge vapor condensation and dissolution, Ge and Au form an alloy and liquefy. The volume of the alloy droplet increases and the elemental contrast decreases, while the alloy composition crosses sequentially, from left to right, a biphasic region (solid Au and Au/Ge liquid alloy) and a single phase region (liquid). An isothermal line in the Au-Ge phase diagram (fig. 2.30b) shows the alloying process.

b) Nucleation as shown fig. 2.29d–e: As the concentration of Ge increases in the Au-Ge alloy droplet, the process of nucleation of the nanowire begins. Knowing the alloy volume change, it is estimated that the nucleation generally occurs at a Ge weight percentage of 50–60%.

c) Axial growth as shown in fig. 2d–f: Once the Ge nanocrystal nucleates at the liquid/solid interface, further condensation/dissolution of the Ge vapor into the system increases the amount of Ge precipitation from the alloy. The incoming Ge vapors diffuse and condense at the solid/liquid interface, thus suppressing secondary nucleation events. The interface is then pushed forward (or backward) to form nanowires (fig. 2.29f). This study confirms the validity of the VLS growth mechanism at the nanometer scale.

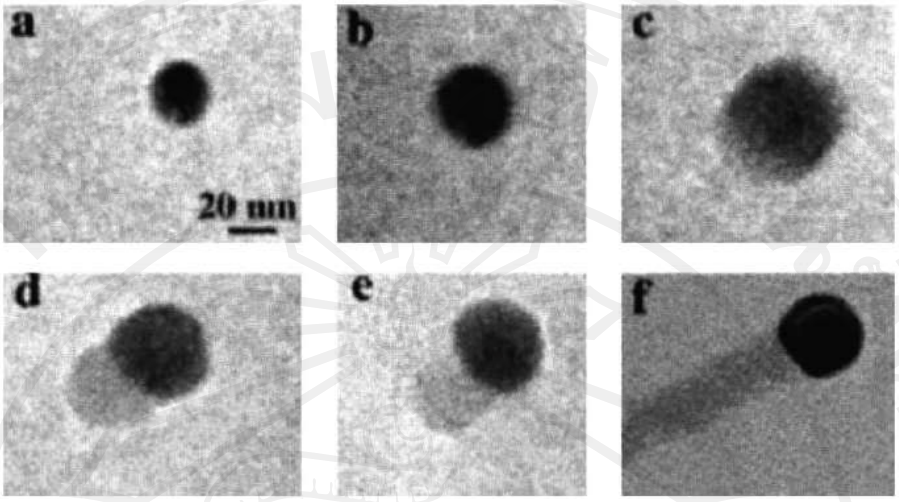

Figure 2.29 In situ TEM images recorded during the process of nanowire growth. a) Au nanoclusters in solid state at 500 °C, b) alloying initiates at 800 °C, at this stage Au exists in mostly solid state, c) liquid Au/Ge alloy; d) the nucleation of Ge nanocrystal on the alloy surface, e) Ge nanocrystal elongates with further Ge condensation and eventually a wire forms f) the interface is pushed forward (or backward) to form nanowires

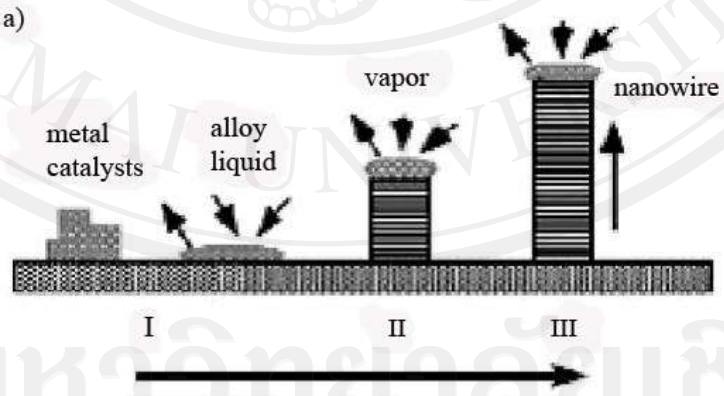

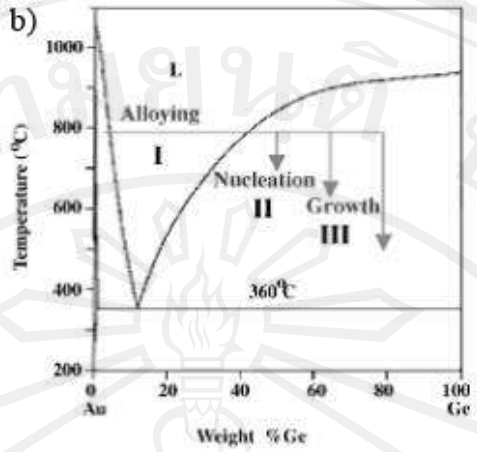

Figure 2.30 a) Schematic illustration of vapor-liquid-solid nanowire growth mechanism including three stages (I) alloying, (II) nucleation, and (III) axial growth. The three stages are projected onto the conventional Au-Ge binary phase diagram, b) shows the compositional and phase evolution during the nanowire growth process

Since the diameter of the nanowires is determined by the diameter of the catalyst particles, this method provides an efficient means to obtain uniform-sized nanowires. Also, with the knowledge of the phase diagram of the reacting species, the Growth temperature can be set in between the eutectic point and the melting point of the material. Physical methods, such as laser ablation or thermal evaporation, as well as chemical methods such as chemical vapor deposition can be used to generate the reactant species in vapor form, required for the nanowire growth. Catalyst particles can be sputtered onto the substrates or metal nanoparticles prepared by solution-based routes used as the catalysts. An advantage of this route is that patterned deposition of catalyst particles yields patterned nanowires. Using this growth mechanism, nanowires of materials including elements, oxides, carbides, phosphides, etc., have been successfully obtained, as detailed in the forthcoming sections.

5. Applications

The great interest that SiC has gathered in latest years is due the possibility to combine in one single material good semiconducting and chemical properties, biocompatibility and sensing potentiality. SiC chemical inertness, wide band gap, tribological properties, hydroxyapatite-like Osseo integration, and hemocompatibility make it a promising candidate for biosensors, interface with biological tissues and lab-on-chip medical devices. Moreover, the possibility to realize nanostructures opens the possibility to assembly novel nanoscale devices and arrays by the bottom-up approach, and to enhance the sensing capabilities of the material.

Several electronic devices, such as power diodes or field-effect transistors based on 3C-SiC (SiCFET) have been developed and SiC power diodes have reached the market stage. Several devices are fabricated by thermally growing SiO_2 layer on n-type Si wafers followed by deposition of parallel Au contacts, used as source and drain electrodes, while the n-type silicon is used as back gate n-type 3C-SiC FETs were tested at different temperatures and were proven to have good performance at high temperatures, with larger current and higher carrier mobility. SiC nanostructures could be used to enhance these landmarks even more, as it happened with other compounds, but very few literature papers deal with SiC NW applications, even if there are already several “proof of concept” nanodevices realized with conventional semiconductors such as Si, GaAs, GaNNW.

Large-scale β-SiCNW coated with SiO_2 layer exhibit the characteristics of an excellent photocatalyst. The photocatalytic activity was evaluated by the photocatalytic decomposition of gaseous acetaldehyde accompanied by generation of carbon dioxide. SiC/ SiO_2 core/shell NW present higher photocatlytic activity than the

pure 3C-SiCNW, resulting from their stronger absorption of gaseous acetaldehyde by SiO_2 and holes remaining in the valence band of SiC.

Organic molecules with different functional groups, such as 3-amine propyl triethoxysilane (APTES) having amine group or mercaptopropyl trimethoxysilane with thiol group, have been suggested for SiCNW surface functionalization. In this framework was used a Supersonic Molecular Beam Deposition approach to functionalize 3C-SiC thick films and NW grown with our VPE reactor. Porphyrins have been deposited onto the SiC surface and the core level/valence band emission has been studied with synchrotron radiation light. First experiments and analysis on SiC film show that both porphyrin macrocycle and the phenyl groups of the molecule have an interaction with the substrate: core level photoemission reveals significant changes on peak positions and line shape. Functionalized 3C-SiCNW shows that oxidized and/or amorphous/oxycarbide components are present, while the Si_{2p} and C_{1s} bands show a strong line shape change. The interaction of attached molecules is more evident on SiCNWs than on films, and a role of F in “etching” the outer shell of NW could be hypothesized.

MEMS are a family of technologies and integrated devices that are becoming more and more important in modern life. Some areas in which these systems are already applied are shock sensors for airbag, inkjet printers, accelerometers and gyroscopes for boats and airplanes, entertainment, healthcare instruments, communication and information technologies, biology and biosensors. MEMS offer significant advantages over hybrid systems and devices because of their small dimensions, integration of different components and low power consumption. Although Si is presently the most used material for MEMS fabrication it has serious

limitations for some applications, such as high temperature (T > 300 °C) and/or harsh environments with corrosive chemicals and biocompatibility, and SiC could be a viable alternative material. Micro cantilever of 3C-SiC with oscillating frequency in the order of 106 Hz and Q factors of 103 were realized and the resonators were used for high sensing applications such as mass detection for gas sensing devices in harsh environment.

Combining MEMS and nanostructures peculiar characteristics such as high affinity to selected species via functionalization and high measurement sensitivity thanks to high resonant frequency and Q factors could open interesting possibility in detection devices for biological applications.

The some preliminary 3C-SiCNW depositions have been made, starting from a patterned Si substrate on which structures such as micron-sized cantilever, beam and springs were fabricated. A Ni layer, nominally 2 nm thick, was deposited as catalyst on this microstructured Si substrate with an e-beam evaporator and the growth was performed in the VPE reactor, using the procedure described above. A SEM micrograph of the NW obtained on the spring is shown in fig. 2.31 [30].

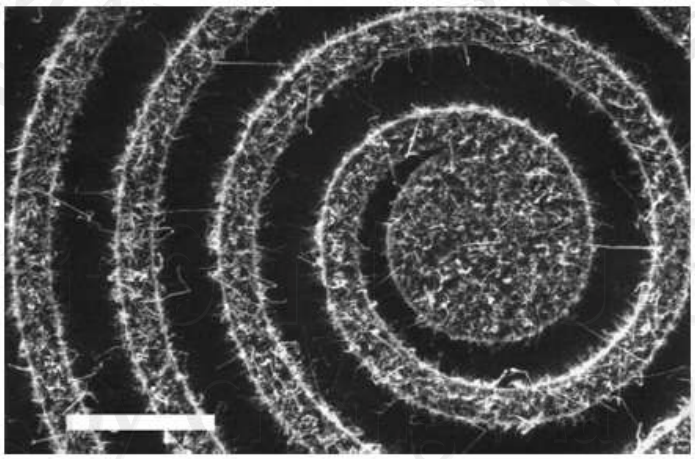

Figure 2.31 SEM micrograph of 3C-SiCNW obtained on a Si spring. Marker is 20 μm [30]